Modeling and simulation of radiation effects in nanometric volumes of silicon and water

M. Batmunkh[2], O. Lkhagva[1,*], L. Bayarchimeg[2], D. Erdenebaatar[1], T. Tuul[1]

[1]*Division of Natural Sciences, National University of Mongolia, Ulaanbaatar*

[2]*Laboratory of radiation biology, Joint Institute for Nuclear Research*

Understanding the effects of particle radiation in nanoscale electronic materials and biological materials is particularly important for future long-term space flights, nuclear medicine and nuclear power plants. Heavy charged particles arriving among galactic cosmic rays have powerful damaging actions when they pass through the electronic devices and biological objects. The present study is focused on the Monte Carlo modeling of stochastic energy depositions in charged particle tracks and calculation of absorbed energy within small sample (200 nm) of silicon and liquid water. The silicon is widely used material for memory chips, computer processors, transistors, and all other electronics. The most common biomaterial is liquid water, which accounts for 60-90% of all living organisms.

The applied simulation technique is based on the Geant4 Monte Carlo transport code, which shows good agreement with experimental cross sections for dosimetry and nano-dosimetry measurements. The calculations were made for protons and carbon ions with different kinetic energies within a relatively wide range of the Bragg curve and linear energy transfer (LET) values from a few to hundreds of keV/μm. We estimated and compared the distribution of energy deposition events and production of reactive chemical species within nanometric volumes of silicon and water after irradiation. We also performed a microdosimetric calculation to estimate LET distribution and nanodosimetric calculation to analyze cluster distributions of ionizations, excitations, elastic collisions and dissociative attachment for electrons corresponds to an interaction with a nonzero energy deposition.

1. INTRODUCTION

Understanding the effects of particle radiation in nanoscale electronic materials and biological materials is particularly important for future long-term space flights, nuclear medicine and nuclear power plants [1]. Currently human exposure is limited to Space Shuttle and International Space Station orbits for which trapped protons are a major concern. However, for interplanetary travel beyond the Earth's magnetosphere, heavy ions in galactic cosmic rays and occasional solar particle events are most significant and powerful damaging actions when they pass through the electronic devices and biological structures. Therefore, study of the radiation sensitivity of small electronic devices and biomaterials ranges from 1-2 to ~ 200 nm is one of the great challenges of studying the biochip resistance to space Environment [2]. The Monte Carlo simulation toolkit Geant4/Geant4-DNA is most suitable computation tool to address this issue and model the microscopic pattern of energy deposition related to an ionizing particle track structure, involving a detailed modeling of the trajectory of all secondary particles with very-low energies [3, 4]. The simulation of single particle track traversing the sensitive volume is the initial event of radiation effects in materials. The effects of radiation in materials depends on the kinetic energy of particle radiation, and some of its energy can be transferred to atoms or molecules, ionization and excitation produces new charged ions, molecules and free radicals. After irradiation, generated chemical species are often highly reactive, and they can decompose or undergo other chemical changes that create a cascade of reactive molecules that may lead to damage biological tissues and other materials. In addition, individual particles can break chemical bonds leading to loss of bases or rupturing of the sugar phosphate backbone of DNA (DeoxyriboNucleic Acid).

The present study is focused on the Monte Carlo simulation of stochastic energy depositions and reactive chemical species in charged particle tracks and calculation of absorbed energy within small sample (200 nm) of silicon and liquid water under irradiation of protons and carbon ions.

2. MATERIAL AND METHODS

The applied simulation technique is based on the Geant4 Monte Carlo transport code [3]. This toolkit is extended to handle microdosimetry and radiobiology applications in the framework of the Geant4-DNA project [4], that is includes the

* Electronic address: olhagvao@yahoo.com

modelling of the three main stages of water radiolysis: (1) the physical stage, describing the elementary physical interactions causing ionized molecules (H_2O^+), excited molecules (H_2O^*) and subexcitations electrons (e_{sub}) spanning from about 10^{-18} s to 10^{-15} s; (2) the physico-chemical stage, being achieved at about 10^{-15} – 10^{-12} s after irradiation and comprising mainly the dissociation or relaxation of water molecules and ions; (3) the chemical stage (10^{-12}–10^{-6} s) describing the diffusion and the reaction of chemical species. The details of the particle track simulation technique implemented in Geant4-DNA are described elsewhere [5]. Such models are restricted to biological materials, liquid water (H_2O) in particular.

Recently, in order to study the sensitivity of advanced electronic devices, down to the nanometer node, Geant4-DNA models extended to other materials, silicon (Si) in particular [6]. The models of theoretical cross sections as Geant4-DNA package for generation of very-low energy (few eV) electrons by incident particles shows good agreement with experimental cross sections for nanodosimetry measurements. The stopping of charged particles in matter is by collisional and radiative processes which occur in frequencies dictated by their interaction cross sections:

$$\left(\frac{dE}{dx} = \int_{E_{cut}}^{E_{max}} \frac{d\sigma}{dE} E dE\right). \qquad (1)$$

In this case, the total cross section, σ is obtained by integrating the single differential cross section between the energy cut-off E_{cut} and the maximum energy that can be transferred to the medium in one single interaction noted as E_{max}. The present study is focused on the simulation of stochastic energy depositions in charged particle tracks and calculation of absorbed energy within small sample (200 nm) of silicon and liquid water. They take into account the production of low energy electrons (E_{cut}) down to 16.7 eV for silicon and 7.8 eV for liquid water. The silicon is widely used material for memory chips, computer processors, transistors, and all other electronics. The most common biomaterial is liquid water, which accounts for 60-90% of all living organisms.

The calculations were made for protons and carbon ions with different kinetic energies within a relatively wide range of Bragg curve and linear energy transfer (LET) values from a few to hundreds of keV/μm. Studying the ability of charged particles to form ionization clusters in a small target plays a central role in the estimation of the damaging capacity of different radiations. Therefore, we performed cluster analysis in track structure of selected particles and estimated the frequency distribution of ionization clusters ($|r_1 - r_2| \leq p$) using the improved K-means approach for space radiobiology problems [7].

In parallel, radiation effect is commonly characterized by microdosimetric quantities such as lineal energy y, its probability density $f(y)$ and dose probability density $d(y)$. The microdosimeter is an important device and technique used to measure and calculate the energy transfer distribution of radiation interacting with a biological system and electronics. In this work, we calculated frequency-mean,

$$\acute{y}_F = \int y f(y) dy\,, \qquad (2)$$

and dose-mean:

$$\acute{y}_D = \frac{\int y^2 f(y) dy}{\acute{y}_F}, \qquad (3)$$

lineal energies from the corresponding distributions of microdosimetric quantities using the part of simulation method [8].

In physics, chemistry and biophysics, the diffusion equation have been widely used to describe the Brownian motion of a molecule in solution and the kinetics of reactions between reactants [9]. The time dependence of the diffusion process may then be described with the help of the three-dimensional Debye-Smoluchowski partial differential equations:

$$\frac{\partial C_i(r,t)}{\partial t} = D_i \nabla^2 C_i(r,t) + R \qquad (4)$$

where $C_i(r,t)$ represent the time dependences of concentration distributions of individual species i, r denoting the position of species, t is time and D_i are corresponding diffusion coefficients. The recombination of water radiolysis, R represents as

$$-C_i(r,t) \sum_j k_{i,j} C_j(r,t) + \sum_{j,k \neq i} k^i_{j,k} C_j(r,t) C_k(r,t). \qquad (5)$$

Here, $k_{i,j}$ are the reaction rate constants for the reaction of the i-th and j-th chemical species. Therefore, we calculated three-dimensional distribution of reactive chemical species using the mentioned diffusion-reaction equation.

3. RESULTS

3.1 Depth dose distribution of charged particles

The depth energy distribution of particle radiation beams during its travel through matter is one of the main factor of radiation dosimetry and nuclear medicine. Energy tranfers of charged particles are commonly expressed as an average energy loss per unit path length and projected range inversely proportional to the square of the charge of the charged particle $\left(\frac{dE}{dx} Z^2_{eff}\right)$. The slowing down of

energetic protons and ions in matter is governed by collisions with the atomic electrons and leads to the characteristic shape of the depth–dose profile of charged particles with a peaking energy deposition, the so-called Bragg peak.

The results of the energy evaluation of 170 MeV protons and 290 MeV/u carbon ions made for silicon and water medium are plotted in Figure 1, 2. Under exposure to protons, the projected range is 105.8 mm in silicon and 197.3 mm in water medium (Figure 1). Energy deposition in silicon more than water, but protons penetration in water more than silicon (Figure 1, b and d). Under exposure to carbon ions, the projected range is 87.5 mm in silicon and 163.2 mm in water medium (Figure 2). Energy deposition of carbon ions in silicon more than water and protons energy distributions (Figure 2, b and d). As this calculations, the energy transfer of particles in nanometer slices at various depth in medium is our special interest. In the following sections, we will estimate the distributions of ionization clusters and lineal energy in nanometer and micrometer samples under exposure to proton and carbon ion with different kinetic energies (blue parts in Figure 1, 2).

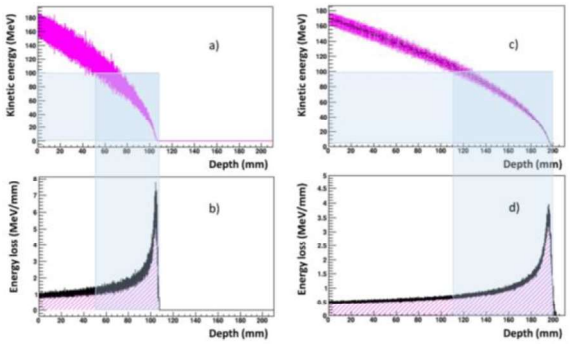

Figure 1. The kinetic energy loss of 170 MeV proton along the particle track in silicon medium (a, b) and water medium (c, d).

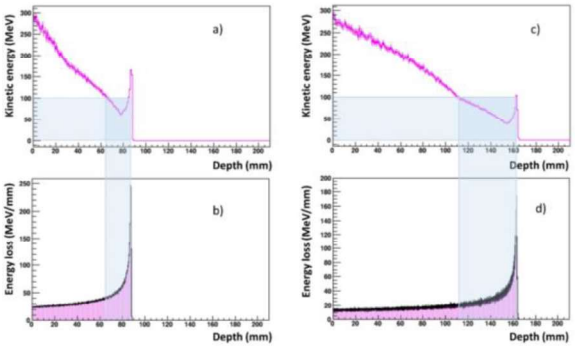

Figure 2. The kinetic energy loss of 290 MeV/u carbon ion along the particle track in silicon (a, b) and liquid water (c, d).

3.2 Scoring of energy deposit in small sample

Single-event effect is the key factor to study the energy transfers of single particle in nanometeric volume with different materials. The energy transfer points were scored in 200 nm voxel, which filled by silicon and liquid water. The results were reported in Figure 3 showing the energy deposition in silicon and water sample under exposure to protons and carbon ions with different kinetic energies. Selected kinetic energies of these particles are respectively corresponding to a range of the Bragg peak (Figure 1 and 2). In the case of proton, more energy absorbed in silicon than water and for carbon ion, more energy absorbed in water than silicon when kinetic energy less than 0.5 MeV/u, respectively.

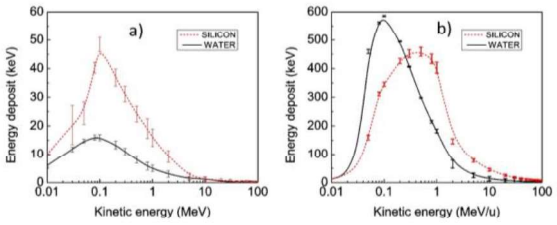

Figure 3. The energy deposition in silicon and water sample (200 nm) under exposure to protons (a) and carbon ions (b) with different kinetic energies, which corresponding to a range of the Bragg peak, respectively.

3.3 Track segment of charged particles at nanometer scale

An example of three-dimensional projections of tracks segment of these particles with same kinetic energy of 1 MeV/u are shown in Figure 4. The energy deposit points are represented as the Cartesian coordinates of the produced physics processes, which corresponds to different interactions with a nonzero energy deposition of ionizations, excitations, elastic collisions, charge changes and electron dissociative attachments for secondary electrons and primary particles. As the results, physical interaction points in water more than silicon for both particles of proton and carbon ion (Figure 3, c and d). However, we obtained more energy deposition in silicon sample than water under irradiation of proton and carbon ion with selected energy (Figure 3).

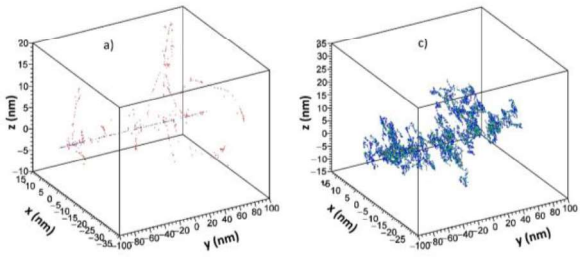

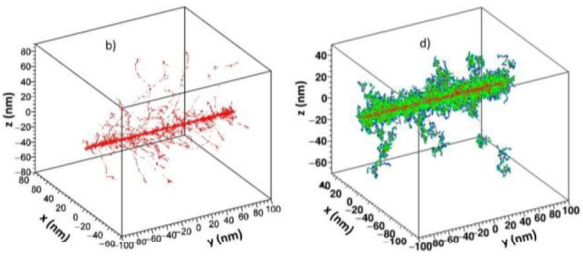

Figure 4. (a, b) - track segment of 1 MeV proton and 1 MeV/u carbon ion in silicon sample with size of 200 nm. Here, red dots are physical interaction events of secondary electrons from incident proton, that`s presents as blue color. Each dots of ionizations, elastic and inelastic collisions, multiple scattering and electron capture for secondary electrons and primary particles corresponds to an interaction with a nonzero energy deposition. (c, d) - track segment of 1 MeV proton and 1 MeV/u carbon ion in water sample with size of 200 nm. Here, each dots represents as different physical processes of ionizations (red), excitations (green), elastic collisions (blue), charge changes (magenta) and electron dissociative attachments (cyan) for secondary electrons and primary particles.

3.4 Nanodosimetric ionization distributions

The standard K-means method is widely used for the analysis of clustering in large datasets. In this work we performed cluster analysis in above track structure of selected particles within small sample using improved clustering algorithm [7]. The results were reported in Figure 5 showing the frequency distribution of ionization clusters in silicon and water sample. In this work, a clustering parameter is estimated to be equal to ~ 3 nm, which is basic length of macromolecules, DNA in particular. Note that cluster order (or cluster size) equals the number of physical interaction points (not only ionization events) within a cluster with diameter of 3 nm. Under exposure to both of proton and carbon ion, frequency distribution of clusters in water higher and broader than silicon (Figure 5). High-order cluster or a cluster with large energy deposition is main factor of clustered DNA damage [10]. Hence, we tried to estimate amounts of DNA damage in water medium.

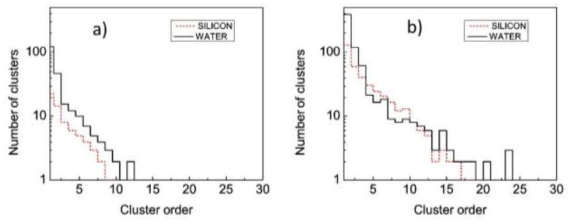

Figure 5. Frequency distributions of clusters with diameter of 3 nm within silicon and water sample (200 nm) under exposure to proton (a) and carbon ion (b) with same energy of 1 MeV/u.

Calculation of clustered DNA damages. In order to estimate amount of clustered DNA damages from the frequency distribution of clusters (Figure 5), threshold value of scored energy deposition within a cluster with diameter of 3 nm is estimated to be about 8.22 eV (excitation energy for water molecule). In Figure 6a, illustrates the frequency distribution of clusters with the energy deposits above the threshold value. As this figure (6b), the occurrence of a lower-order cluster (< 5) is more probability for only ionization events rather than for all interaction events. Hence, energy deposition of a cluster more than a threshold value, it leads to single strand break (SSB). Two SSBs are considered a double strand break (DSB) if they are located within a cluster volume corresponding distance to DNA segments of 10 base pairs. Under exposure to 1 MeV single proton in water sample (200 nm), number of SSB and DSB is 20 and 9, ratio of total strand breaks is calculated about 2.21 of simple SSB/DSB. In the case of 1 MeV/u carbon ion, number of SSB and DSB is 139 and 62, ratio of total strand breaks is calculated about 2.25 of simple SSB/DSB. In figure 7, illustrated distribution of clustered SSB and DSB in track structure of chosen particles. Note that we also compared results from K-means approach [7] with calculations of Goodhead (2015) [10] for 2 MeV alpha particle in liquid water. In this case, ratio of strand breaks is 2 and ~1.5 of SSB/DSB, 27 and ~24 of SSB complex/simple (%), 73 and ~71 of DSB complex/simple (%).

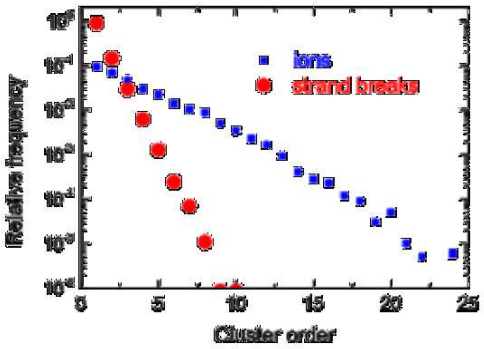

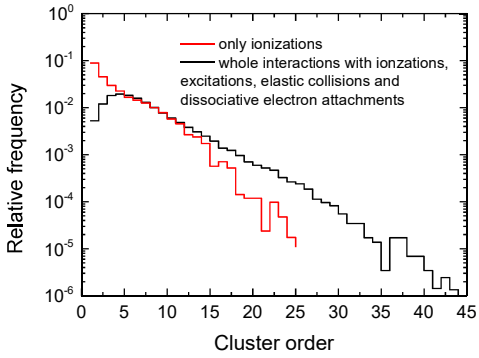

Figure 6. Frequency distribution of clusters with energy more than zero and threshold value for 1 MeV proton (a). Comparison of only ionizantion events and all interaction processes for 1 MeV/u carbon ion (b).

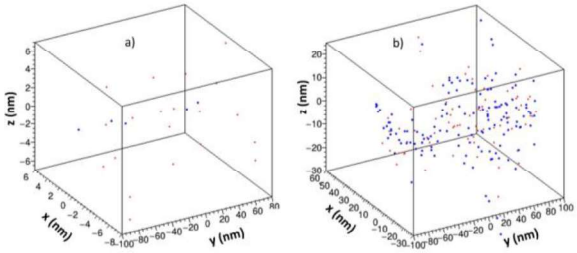

Figure 7. Distribution of clustered DNA SSB (red) and DSB (blue) along the track structure of 1 MeV proton (a) and 1 MeV/u carbon ion in water sample. The track structure represented from Figure 4.

3.5 Microdosimetric energy distributions

In this section, described some of the numerical calculations of basic microdosimetric quantities for particles that are generally used in hadrontherapy, mainly protons and carbon ions, taking into account the secondary electrons tracks that are generated in tissue-like media (liquid water). The specific energy and the lineal energy transfer are stochastic quantities and their distributions can be of importance for radiation quality assessment. The results were reported in Figure 8 showing the plot of lineal energy y, its probability density f(y) for proton and carbon ions with same energy of 1 MeV/u in silicon and water sample. Here, the number of sampling per incident event is 1000 and sample size is 3 um. Under exposure to proton, lineal energy in silicon is broader and higher frequently than water sample (Figure 8a). Under exposure to carbon ion, lineal energy in water is broader than in silicon (Figure 8b). In the case of water sample, first peak is corresponding to delta rays as secondary electrons and second peak corresponds to track core of primary particle. Hence, we calculated frequency-mean, $\acute{y}_f$, and dose-mean, $\acute{y}_D$, lineal energies from the corresponding distributions of microdosimetric quantities using the simulation method [8]. In the case of proton, $\acute{y}_f = 146\,eV/nm$ and $\acute{y}_D = 160.4\,eV/nm$ in silicon sample, $\acute{y}_f = 57.6\,eV/nm$ and $\acute{y}_D = 66.5\,eV/nm$ in water sample. In the case of carbon ion, $\acute{y}_f = 2499\,eV/nm$ and $\acute{y}_D = 2713\,eV/nm$ in silicon sample, $\acute{y}_f = 1304\,eV/nm$ and $\acute{y}_D = 2200\,eV/nm$ in water sample.

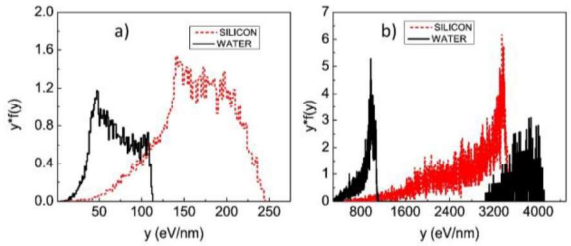

Figure 8. Lineal energy spectrum for proton (a) and carbon ion (b) with same energy of 1 MeV/u irradiating the silicon and water medium.

3.6 Mathematical modeling and computer simulation of water radiolysis

Throughout this article, the physico-chemical (10^{-15}–10^{-12} s) and chemical (10^{-12}–10^{-6} s) stages in the track development are simulated in terms of diffusion and interaction of the most widespread products of water radiolysis including the solvated electrons e^-_{aq}, hydroxyl radical $^{\bullet}OH$, hydronium ion H_3O^+, hydrogen radical $H^{\bullet}$, hydroxide ion OH^-, dihydrogen H_2, and hydrogen peroxide H_2O_2. The production of these species is originated by the physical stage (10^{-18}–10^{-15} s) where the energy deposition by incident particles and by secondary electrons occurs through the slowing down of the particles via a variety of elastic collision processes, including ionization, electronic and vibrational excitation of single water molecules, and dissociative electron attachment. In Table 1, represented chemical reactions of basic water radiolysis [11]. These physico-chemical and chemical stages are simulated with Geant4-DNA processes, using the default values of branching ratios, diffusion coefficients, reaction rates and time steps [5, 12].

In order to calculate space and time evolution of additional reactive chemical species beyond the microsecond after irradiation we used analytic solution of Debey-Smolochowski diffusion equation (see in Materials and Methods). Hence, were converted to systems of ordinary differential equations from the chemical reactions (Table 1). The results were reported in Figure 9 showing the theoretical 3D Smoluchowski solution of water

radiolysis, solvated electron e_{aq}^{-} in particular at 1ns, 10 ns and 100 ns of chemical stage. In this work, we compared the distribution of diffusion at 1 ns and 1 μs from the theoretical 3D Smoluchowski solution of water radiolysis with Geant4-DNA Monte Carlo simulation results. Figure 10 shows small portions of proton and carbon ion tracks with the most important radiolytic species (e^{-}_{aq}, $^{\bullet}OH$, H_3O^+, $H^{\bullet}$, OH^-, H_2, and H_2O_2.) and their locations in water sample at 1 ns of the chemical stage (10^{-9} s). The concentration of created species traversed the water sample presented in Figure 11. The concentration was calculated as the $N/N_A \bullet V$, where N is number of molecular species, N_A is avogadro's constant and V is volume of 200 nm water sample. According to the results, the solvated electrons e^{-}_{aq} and hydronium ion H_3O^+ for both particles are high-frequently traversed the small sample. Contrariwise, the yield of hydroxide ion OH^- is most lower observed at 1 ns after irradiation of both particles. For 1 MeV proton irradiation, the concentration of e^{-}_{aq}, $^{\bullet}OH$, H_3O^+, $H^{\bullet}$, OH^-, H_2, and H_2O_2 species at the 1 ns of the chemical stage, respectively, 16.2-, 9.2-, 17.1-, 17.5-, 30.5-, 57.2- and 63.7-times lower than carbon ion irradiation. Under exposure to carbon ion, the hydrogen peroxide (H_2O_2) is more generated than hydroxyl radical $^{\bullet}OH$ at 1 ns (Figure 11b).

Table 1. (a) List of considered reactive species and corresponding diffusion coefficients D. (b) List of considered reactions and corresponding reaction rate constants k.

a)

Species	D ($\times 10^{-9}$ m^2 s^{-1})
e^{-}_{aq}	4.9
$^{\bullet}OH$	2.8
$H^{\bullet}$	7.0
H_3O^+	9.0
H_2	4.8
OH^-	5.0
H_2O_2	2.3

b)

Reaction	k (M^{-1}s^{-1})
$e^{-}_{aq} + e^{-}_{aq} + 2H_2O \longrightarrow H_2 + 2OH^-$	0.50×10^{10}
$e^{-}_{aq} + {}^{\bullet}OH \longrightarrow OH^-$	2.95×10^{10}
$e^{-}_{aq} + H^{\bullet} + H_2O \longrightarrow H_2 + OH^-$	2.65×10^{10}
$e^{-}_{aq} + H_3O^+ \longrightarrow H^{\bullet} + H_2O$	2.11×10^{10}
$e^{-}_{aq} + H_2O_2 \longrightarrow OH^- + {}^{\bullet}OH$	1.41×10^{10}
$^{\bullet}OH + {}^{\bullet}OH \longrightarrow H_2O_2$	0.44×10^{10}
$^{\bullet}OH + H^{\bullet} \longrightarrow H_2O$	1.44×10^{10}
$H^{\bullet} + H^{\bullet} \longrightarrow H_2$	1.20×10^{10}
$H_3O^+ + OH^- \longrightarrow 2H_2O$	1.43×10^{11}

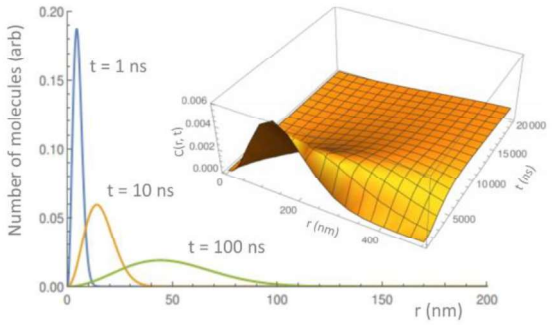

Figure 9. The analytic solution of 3D Smoluchowski PDEs for solvated electron diffusion at 1 ns, 10 ns and 100 ns.

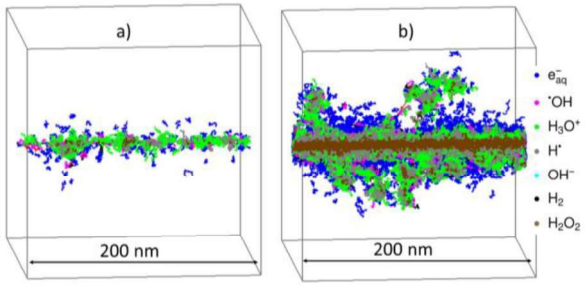

Figure 10. The chemical stage of proton and carbon ion track with 1 MeV/u energy in water sample at reaction time of 1 ns with Geant4-DNA models. The physical stage of particle tracks at 1 fs shown in Figure 4.

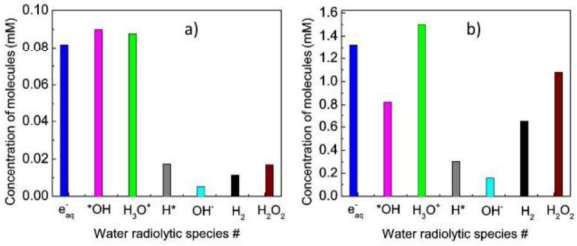

Figure 11. The concentration of basic water radiolysis for proton (a) and carbon ion (b) with 1 MeV/u energy in water sample at reaction time of 1 ns with Geant4-DNA models.

4. RESULTS AND DISCUSSION

In this work we have considered a theoretical model for description of cluster growth in C_{60}/NMP solutions. The stationary distribution functions were calculated and used for modeling of the small angle neutron scattering curves. The results of spectral analysis give cluster sizes of fullerene in NMP solutions at range 3.5-100 nm.

Investigations of kinetics of fullerene dissolution and complex formation were performed for low-polar and polar solvents at different preparation conditions. For low-polar solutions, the dissolution is well described by Noyes-Whitney equation. For polar solutions we had to extend dissolution equations to account for the complex formation. The

dependence of kinetic parameters on different preparation conditions was obtained.

Investigation of structural properties of C_{70} in CS_2 solutions was performed at the SANS instrument in FLNP JINR, Dubna. The solutions were prepared at different conditions. The experimental results were compared to measurements by other groups.

ACKNOWLEDGEMENTS

This work was supported by the Russian Foundation for Basic Research, project No.14-23-01015. The financial support is gratefully acknowledged.

REFERENCES

[1] Beck M.T., Mandi, G., Fullerene Sci. and Technol., 5(2), 291-310, 1997.

[2] Kyzyma, O.A., Korobov, M.V., Avdeev, M.V., Garamus, V.M., Petrenko, V.I., Aksenov, V.L., Bulavin, L.A., Fullerenes, Nanotubes and Carbon Nanostructures, 18, 458-461, 2010.

[3] M.V. Avdeev, V.L. Aksenov, T.V. Tropin, "Models of cluster formation and growth in fullerene solutions," Russ. J. Physical Chemistry A, 84(8), 1273-1283, 2010.

[4] K.A. Affholter, S.J. Henderson, et al., "Structural characterization of C_{60} and C_{70} fullerenes by small- angle neutron scattering," J. Chem. Phys., vol. 99, no. 11, pp. 9224-9229, 1993.

[5] S.J. Henderson, Measurement of the Second Virial Coefficient of C_{60} in CS_2 Solution from Small-Angle Neutron Scattering, Langmuir. 13 6139–6145, 1997.

[6] M. V. Avdeev, T. V. Tropin, I.A. Bodnarchuk, S.P. Yaradaikin, L. Rosta, V.L. Aksenov, et al., On structural features of fullerene C_{60} dissolved in carbon disulfide: complementary study by small-angle neutron scattering and molecular dynamic simulations., J. Chem. Phys. 132 164515, 2010.

[7] T.V. Tropin, N. Jargalan, et al., "Kinetics of cluster growth in polar solutions of fullerene: Experimental and theoretical study of C_{60}/NMP solution," J. Mol. Liq., 175, 4, 2012.

[8] A.A. Noyes, W.R. Whitney, "The rate of solution of solids substances in their own solutions," J. Am. Chem. Soc., 19(12), 930, 1897.